

Seasonal Variations of Soil Thermal Conductivity at the InSight Landing Site

M. Grott¹, S. Piqueux², T. Spohn^{1,3}, J. Knollenberg¹, C. Krause⁴, E. Marteau², T.L. Hudson², F. Forget⁵, L. Lange⁵, N. Müller¹, M. Golombek², S. Nagihara⁶, P. Morgan⁷, J.P. Murphy⁸, M. Siegler^{9,10}, S.D. King⁸, D. Banfield¹¹, S.E. Smrekar², W.B. Banerdt²

¹German Aerospace Center (DLR), Institute of Planetary Research, Berlin, Germany

²Jet Propulsion Laboratory, California Institute of Technology, Pasadena, USA

³International Space Science Institute (ISSI), Bern, Switzerland

⁴German Aerospace Center (DLR), MUSC Space Operations and Astronaut Training, Cologne, Germany

⁵Laboratoire de Météorologie Dynamique (LMD/IPSL/CNRS), Sorbonne Université, Paris, France

⁶Department of Geosciences, Texas Tech University, Lubbock, USA

⁷Colorado Geological Survey, Colorado School of Mines, Golden, USA

⁸Virginia Polytechnic Institute and State University, Blacksburg, USA

⁹Planetary Science Institute, Tucson, AZ, USA

¹⁰Southern Methodist University, Dallas, TX, USA

¹¹Cornell University, Ithaca, New York, USA

Key Points:

- We measured thermal conductivity of the martian soil and found that its conductivity strongly correlates with atmospheric pressure.
- We conclude that heat conduction through the pore-filling gas is significant and that cementation of the soil must be minimal.
- Our data show that the atmosphere directly interacts with the top most meter of material on Mars.

25 **Abstract**

26 The heat flow and physical properties package measured soil thermal conductivity at the
 27 landing site in the 0.03 to 0.37 m depth range. Six measurements spanning solar longi-
 28 tudes from 8.0° to 210.0° were made and atmospheric pressure at the site was simulta-
 29 neously measured using InSight's Pressure Sensor. We find that soil thermal conductiv-
 30 ity strongly correlates with atmospheric pressure. This trend is compatible with predic-
 31 tions of the pressure dependence of thermal conductivity for unconsolidated soils under
 32 martian atmospheric conditions, indicating that heat transport through the pore filling
 33 gas is a major contributor to the total heat transport. This implies that any cementa-
 34 tion or induration of the soil sampled by the experiments must be minimal and that the
 35 soil surrounding the mole at depths below the duricrust is unconsolidated. Thermal con-
 36 ductivity data presented here are the first direct evidence that the atmosphere interacts
 37 with the top most meter of material on Mars.

38 **Plain Language Summary**

39 A soil's ability to transport heat is a fundamental parameter that holds informa-
 40 tion on quantities like soil bulk porosity, composition, grain size, and the state of cemen-
 41 tation or induration. In the soil, heat is transported through grain-to-grain contacts as
 42 well as through the pore filling CO₂ gas. The heat flow and physical properties pack-
 43 age (HP³) of the InSight Mars mission measured soil thermal conductivity at the land-
 44 ing site repeatedly over the course of a martian year. As atmospheric pressure changes
 45 between seasons due to the redistribution of CO₂ across the planet, we found that soil
 46 thermal conductivity also changes. Thermal conductivity increased for increased atmo-
 47 spheric pressure, a behaviour typical for unconsolidated material. This implies that the
 48 amount of cement or induration of the sampled soil must be minimal.

49 **1 Introduction**

50 Thermal conductivity is a fundamental physical property that largely controls the
 51 range of temperatures experienced at the surface and in the shallow subsurface of a planet.
 52 In granular material, heat is transported through grain-to-grain contacts, conduction through
 53 the pore-filling gas, and radiation between individual grains. In martian soil, the first
 54 two contributions dominate the transport, and grain-to-grain contacts are particularly
 55 enhanced if grains are cemented or indurated (Presley et al., 2009; Piqueux & Christensen,

56 2009b). Conversely, the contribution of heat transport through the gas phase can inform
 57 us about the state of soil cementation or induration.

58 For grain sizes between a few tens of μm and a few mm (Hamilton et al., 2014; Fer-
 59 gason et al., 2006; Edgett et al., 2013; Yingst et al., 2013) and atmospheric pressures of
 60 a few mbar typically encountered on Mars, the mean free path of gas molecules is sim-
 61 ilar to pore size and gas flow occurs in the transitional flow regime (Piqueux & Chris-
 62 tensen, 2009a). This results in a strong dependence of soil thermal conductivity on at-
 63 mospheric pressure (Presley & Christensen, 1997; Huetter et al., 2008; Nagihara et al.,
 64 2022) in unconsolidated material, whereas conduction through the gas phase becomes
 65 less important when the soil is cemented or indurated, where conduction mainly occurs
 66 through the soil matrix (Piqueux & Christensen, 2009b).

67 The only in-situ thermal measurements of the martian soil using transient heat-
 68 ing methods were performed by the thermal and electrical permittivity probe (TECP)
 69 during the Phoenix mission (Mellon et al., 2009; Zent et al., 2010) and those taken by
 70 the heat flow and physical properties package (HP³) on the InSight mission (Banerdt et
 71 al., 2020; Spohn et al., 2018; Grott et al., 2019, 2021). The Phoenix measurements in
 72 Vastitas Borealis at 68.22°N 234.25°E, as well as the InSight measurements in Elysium
 73 Planitia at 4.50°N, 135.62°E, both showed that the martian soil is a poor thermal con-
 74 ductor. Thermal conductivity at the Phoenix site was determined to be 0.085 W m^{-1}
 75 K^{-1} in the upper 1.5 cm of the soil (Zent et al., 2010), while an average thermal con-
 76 ductivity of $0.039 \pm 0.002 \text{ W m}^{-1} \text{ K}^{-1}$ was determined for the upper 37 cm of the soil
 77 column at the InSight landing site (Grott et al., 2021). The difference between the two
 78 measurements has been attributed to the presence of cementing agents like perchlorate
 79 salts (Grott et al., 2021), which are abundant at the polar Phoenix landing site (Hecht
 80 et al., 2009; Kounaves et al., 2014).

81 To study the relative importance of grain-to-grain as well as gas conduction in the
 82 martian soil, measurements at different atmospheric pressures are needed. However, due
 83 to the Phoenix mission's limited lifetime, such measurements could not be made. Here
 84 we report on the first long term monitoring of soil thermal conductivity as a function
 85 of atmospheric pressure as derived from in-situ measurements at the InSight landing site.

86 2 Probe Emplacement, Data Acquisition and Inversion

87 Following deployment onto the martian surface, HP³ started its first penetration
 88 attempt on Sol 92 of the mission (February 28, 2019). However, insufficient friction to
 89 compensate for recoil during hammering resulted in an initial failure to penetrate (Spohn
 90 et al., 2022; Spohn et al., 2022). Further penetration was only possible after removing
 91 the HP³ support structure and using the lander's robotic arm to provide friction by di-
 92 rectly interacting with the HP³ mole. In this way, it was possible to reach a mole depth
 93 of approximately 3 cm below the surface as measured from the mole's back cap. Following
 94 penetration, the hole behind the mole was filled with scraped soil which was tamped down
 95 to ensure that the mole was fully buried and in contact with soil. A first thermal con-
 96 ductivity measurement with a fully buried mole was conducted on Sol 680 of the mis-
 97 sion and a final hammering attempt was conducted on Sol 754. However, no additional
 98 depth progress was observed and further penetration attempts were abandoned.

99 The final burial of the HP³ mole is shown in Fig. 1a and thermal conductivity was
 100 measured in this configuration when energy could be made available on the lander. Six
 101 measurements were conducted on Sols 798, 827, 874, 1070, 1160, and 1204, correspond-
 102 ing to solar longitudes L_s of 8.0°, 22.0°, 44.2°, 135.3°, 184.0°, and 210.0°, where L_s is
 103 defined as the aerocentric longitude measured from the northern hemisphere spring equinox
 104 where $L_s = 0^\circ$. During the measurements, the mole was used as a modified line heat
 105 source (Hammerschmidt & Sabuga, 2000; Spohn et al., 2018) and a specified constant
 106 heating power was provided to the mole's outer hull. Thermal conductivity was then de-
 107 termined from the resulting temperature rise of the mole hull as a function of time (Spohn
 108 et al., 2018). Before each active heating experiment was started, background temper-
 109 ature drift was monitored for 2 Sols and the average was subtracted from the measure-
 110 ments to obtain the heating-induced temperature rise from which conductivity was de-
 111 termined (see Grott et al. (2021) for details).

112 A schematic cross section of the soil surrounding the mole, which has been derived
 113 based on geologic observations (Golombek, Williams, et al., 2020) and the history of probe
 114 emplacement (Spohn et al., 2022), is shown in Fig. 1b. It includes a layer of unconsol-
 115 idated surfacial dust and sand as well as a hole surrounding the back of the mole, which
 116 has been back-filled by scraping unconsolidated material followed by taping the soil down
 117 using the robotic arm's scoop. Furthermore, the duricrust as inferred from image and

Figures/Fig1.pdf

Figure 1. (a) Configuration of the HP³ mole after the final penetration attempts on Sol 754 of the mission. During final hammering, the robotic arm's scoop pressed onto the ground (note the smooth rectangular imprint) to provide support and increase pressure on the mole hull. The scoop also acted as a safeguard to prevent the mole from recoiling backwards. The image was taken after retraction of the robotic arm on Sol 755. (b) Schematic cross section of the soil surrounding the mole indicating a surfacial dust and sand layer over a duricrust and unconsolidated sand. The hole around the back of the mole was back-filled with cohesionless material and tamped down. The volume of soil sampled by the thermal conductivity experiments as well as the region of potentially disrupted soil is indicated.

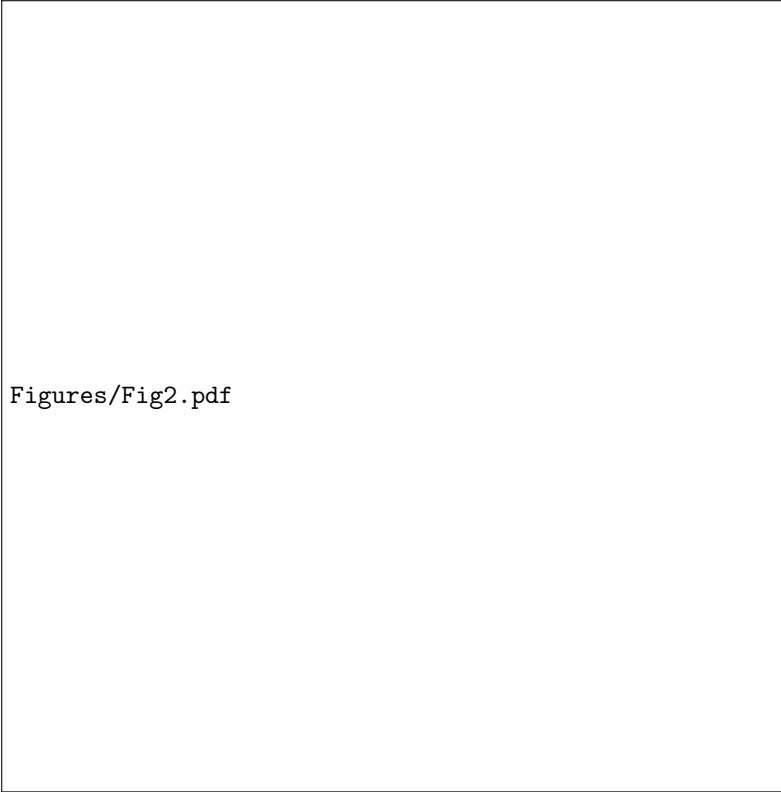


Figure 2. Temperature rise as a function of heating time t for all measurements performed in the fully buried, final mole configuration. The inset shows details of the log-linear regime between 2 and 10 hours after the start of the measurements.

penetration data is indicated. At larger depth, the soil is inferred to be unconsolidated. The soil volume sampled by the experiments is indicated in red shades and the generated heat pulse has a diffusion length scale of $d_\epsilon = \sqrt{kt/\rho c_p}$. Assuming a thermal conductivity of $k = 0.0385 \text{ W m}^{-1} \text{ K}^{-1}$, density ρ of 1211 kg m^{-3} , and heat capacity c_p of $630 \text{ J kg}^{-1} \text{ K}^{-1}$, $d_\epsilon \approx 6.2 \text{ cm}$ for the 21 h 40 min heating experiment. The volume of soil sampled during the experiment extends to 2 to 3 mole diameters and is thus considerably larger than the region of potentially disrupted soil (also compare Fig. 3 in Grott et al. (2021)). Note that the presence of a gravel layer around of the tip of the mole has been derived based on the mole's penetration performance (Spohn et al., 2022) but is not shown here. The tilt of the mole with respect to the local gravity vector is close to 30° .

The retrieved temperature rise as a function of time t is shown for all six thermal conductivity measurements in Fig. 2 and all measurements were performed in the final

131 mole configuration with no hammering in between. Heating curves followed a similar trend,
 132 showing the classical log-linear increase of temperature as a function of $\log(t)$ at inter-
 133 mediate heating times between 2 and 10 hours before axial heat flow causes a deviation
 134 at later times.

135 For a classical line heat source, the slope of the heating curve $dT/d\log(t)$ is inversely
 136 proportional to the thermal conductivity of the medium. Therefore a first qualitative con-
 137 clusion concerning the pressure dependence of thermal conductivity at the InSight land-
 138 ing site can be already drawn from inspection of the slopes in Fig. 2. In the figure, large
 139 slopes are associated with Sols of low atmospheric pressure and vice versa (compare Ta-
 140 ble 1), which implies that soil thermal conductivity and atmospheric pressure are pos-
 141 itively correlated. This conclusion is supported by analytical models (Jaeger, 1956; Carslaw
 142 & Jaeger, 1959; Hammerschmidt & Sabuga, 2000) and a linear analysis roughly repro-
 143 duces the trends reported below (see supplemental material). However, using the clas-
 144 sical line heat source approach (von Herzen & Maxwell, 1959), thermal conductivities
 145 are slightly overestimated due to the fact that axial heat flow cannot be accounted for
 146 in these models (Blackwell, 1956).

147 Therefore, we rely on numerical models to invert the heating curves for soil ther-
 148 mal conductivity k . The model accounts for the non-negligible specific heat of the mole,
 149 the contact conductance H between mole and regolith as well as the geometry of the prob-
 150 lem including axial heat transport. It is described in detail in Spohn et al. (2018) and
 151 Grott et al. (2019, 2021), and we used a Monte-Carlo approach to find admissible sets
 152 of model parameters k and H which fit the observations. While thermal conductivity
 153 k as well as contact conductance H change as a function of atmospheric pressure, den-
 154 sity ρ remains unaffected and we require the numerical model to fit measurements at dif-
 155 ferent seasons using a fixed density.

156 For each model run, modeled temperature $T_{mod}(t, k, H)$ is compared to the mea-
 157 sured temperature rise $T_{dat}(t)$ and the root mean square deviation between the two quan-
 158 tities is determined according to

$$\Delta T_{rms}(k, H) = \left(\sum_{i=1}^n (T_{mod}(t_i, k, H) - T_{dat}(t_i))^2 / n \right)^{\frac{1}{2}} \quad (1)$$

159 Here $n = 1000$ is the number of measurement points. Following Grott et al. (2021), data
 160 were inverted between $t_1 = 1$ h and $t_n = 21$ h 40 min. Admissible parameter sets (k, H)
 161 were then determined by requiring the root mean square deviation $\Delta T_{rms}(k, H)$ to be

162 smaller than 0.17 K. This threshold takes the observed day-to-day temperature varia-
 163 tions as well as other sources of uncertainty into account (see Grott et al. (2021) for de-
 164 tails). As the soil density was not known a priori, we ran two different sets of inversions
 165 using the two median densities derived for the InSight landing site by Grott et al. (2019).
 166 These are $\rho = 1007 \text{ kg m}^{-3}$ and $\rho = 1211 \text{ kg m}^{-3}$, where the latter corresponds to
 167 an estimate that includes the additional constraint posed by the surface thermal iner-
 168 tia as derived from HP³ radiometer measurements (Mueller et al., 2020, 2021). For the
 169 soil specific heat capacity, a value of $630 \text{ J kg}^{-1} \text{ K}^{-1}$ has been assumed (Morgan et al.,
 170 2018). 20,000 Monte-Carlo simulations were then run for each of the measurements per-
 171 formed on Sol 798, 827, 874, 1070, 1160, and 1204. In the simulations, thermal conduc-
 172 tivity k and contact conductance H were drawn from uniform probability distributions
 173 spanning the range $0.034 < k < 0.042 \text{ W m}^{-1} \text{ K}^{-1}$ and $3 < H < 250 \text{ W m}^{-2} \text{ K}^{-1}$,
 174 respectively.

175 A discussion of measurement uncertainty associated with the determination of ther-
 176 mal conductivity from HP³ measurements is given in Grott et al. (2019) and Grott et
 177 al. (2021). However, for the present analysis, we are searching for relative changes in ther-
 178 mal conductivity only, such that systematic sources of uncertainty which are identical
 179 for all measurements can be neglected. These include the uncertainties associated with
 180 determining the heat input into the TEM-A foils, the uncertainty associated with the
 181 imperfections of the finite element model, as well as the uncertainty of the reference method
 182 (Grott et al., 2021). Only the contribution stemming from the allowable spread of mod-
 183 els determined using the Monte-Carlo simulations needs to be considered, and error bars
 184 stated below refer to the $1-\sigma$ standard deviations of the admissible model parameters.

185 Atmospheric pressure at the InSight Landing site has been measured at a cadence
 186 of 20 Hz by the Pressure Sensor (PS) of the InSight Auxiliary Payload Sensor Suite (APSS)
 187 (Banfield et al., 2019, 2020; Spiga et al., 2018), and we here use the most recent recal-
 188 ibrated dataset as provided by Lange et al. (2022). Diurnal average surface atmospheric
 189 pressure P can be approximated by

$$P = a_0 + \sum_{n=1}^6 a_n \cos(nL_s) + b_n \sin(nL_s) \quad (2)$$

190 where the coefficients are given in units of Pascals and $a_0 = 721.5$, $a_1 = 36.99$, $a_2 =$
 191 -34.57 , $a_3 = -0.6312$, $a_4 = -0.3281$, $a_5 = 0.1213$, $a_6 = 0.6940$, $b_1 = -33.99$, $b_2 =$
 192 36.77 , $b_3 = -0.6382$, $b_4 = -3.655$, $b_5 = 0.6656$, and $b_6 = 0.8195$. L_s is solar longitude

193 in degrees. Average diurnal atmospheric pressure at the landing site is thus found to vary
 194 between 6.25 and 7.95 mbar.

195 Soil thermal conductivity corresponding to the above atmospheric pressures can
 196 be estimated using the model of Morgan et al. (2018), which is based on a parameter-
 197 ization of laboratory experiments on unconsolidated soil performed by Presley & Chris-
 198 tensen (1997). Given the soil thermal conductivity $k_0(P)$ at atmospheric pressure P , ther-
 199 mal conductivity at pressure $P + \Delta P$ can be calculated from

$$k(P + \Delta P) = k_0(P)(1 + A\Delta P + B\Delta P^2) \quad (3)$$

200 where ΔP is the atmospheric pressure deviation with respect to P in mbar. The fitting
 201 constants A and B are given by 5.173 mbar^{-1} and $-0.2416 \text{ mbar}^{-2}$, respectively (Mor-
 202 gan et al., 2018).

203 3 Results

204 Results of the simulations are summarized in Table 1, where the Sol number, mar-
 205 tian solar longitude L_s , soil temperature at the beginning of the experiment T_0 , aver-
 206 age (P_{avr}), minimum (P_{\min}) and maximum (P_{\max}) atmospheric pressure during the mea-
 207 surement, as well as soil density ρ are given together with the derived thermal conduc-
 208 tivity k . A clear correlation between atmospheric pressure and soil thermal conductiv-
 209 ity is evident. Results are insensitive to the chosen soil density, and derived soil ther-
 210 mal conductivities for the two sets of simulations using $\rho = 1007 \text{ kg m}^{-3}$ and $\rho = 1211$
 211 kg m^{-3} are indistinguishable within their respective error bars. It is worth noting that
 212 in principle the temperature dependence of heat capacity and soil matrix thermal con-
 213 ductivity could account for some of the seasonal variations observed in the inverted ther-
 214 mal conductivities. However, because there is no correlation between soil temperature
 215 T_0 and thermal conductivity k in Table 1, such an effect can be ruled out. Also, a di-
 216 rect influence of the observed seasonal trend on the variations of seismic velocities as re-
 217 ported by Compaire et al. (2022) is unlikely for the same reason.

218 Soil thermal conductivity for the case $\rho = 1211 \text{ kg m}^{-3}$ is shown in Fig. 3 as a
 219 function of martian solar longitude L_s for the measurements taken on sols 798, 827, 874,
 220 1070, 1160 and 1204, corresponding to $L_s = 8.0^\circ, 22.0^\circ, 44.2^\circ, 135.3^\circ, 184.0^\circ$, and 210.0° ,
 221 respectively. Measurements roughly span $\sim 60\%$ of a martian year while covering $\sim 85\%$
 222 of the encountered pressures. To compare the obtained results with conductivities ex-

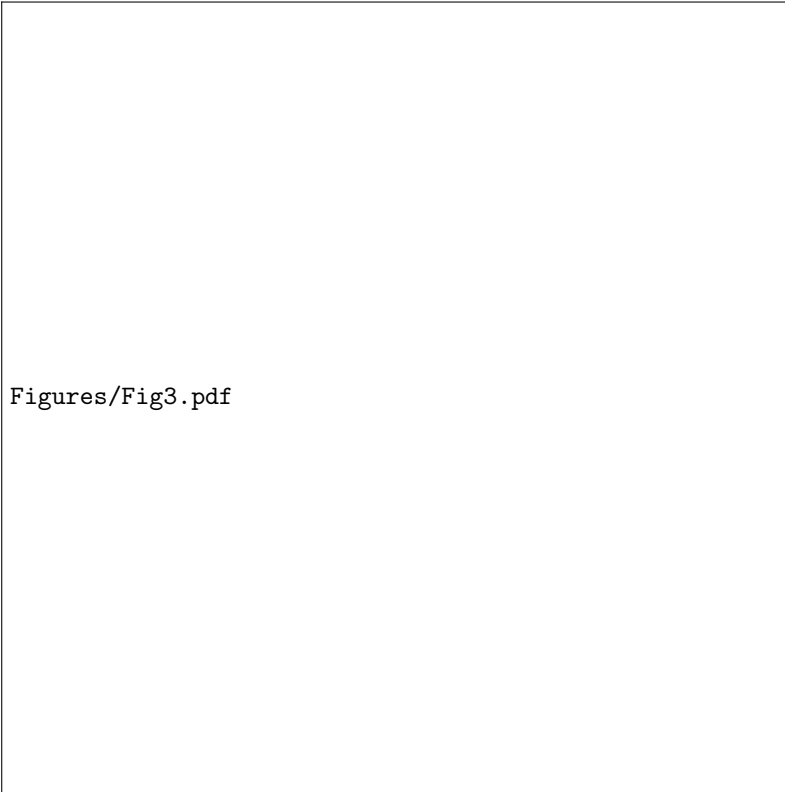


Figure 3. Thermal conductivity as a function of martian season assuming $\rho = 1211 \text{ kg m}^{-3}$. Six active heating experiments were conducted over the period of $L_s = 8.0^\circ$ to $L_s = 210^\circ$ before the reduction of solar power on the InSight lander prevented further measurements to be taken towards the end of the mission. A model of thermal conductivity as a function of atmospheric pressure is shown for reference (Morgan et al., 2018). Here, the solid line corresponds to average diurnal atmospheric pressures and the gray shaded area shows the expected range of thermal conductivity including diurnal pressure fluctuations.

Sol	L_s [°]	T_0 [K]	P_{avr} [mbar]	P_{min} [mbar]	P_{max} [mbar]	ρ [kg m ⁻³]	k [W m ⁻¹ K ⁻¹]
798	8.0	222.02	7.30	7.07	7.52	1007	0.0383 ± 0.0007
827	22.0	220.26	7.44	7.20	7.65	1007	0.0395 ± 0.0007
874	44.2	217.75	7.61	7.39	7.75	1007	0.0397 ± 0.0007
1070	135.3	218.61	6.39	6.21	6.53	1007	0.0366 ± 0.0007
1160	184.0	225.37	6.60	6.35	6.89	1007	0.0371 ± 0.0006
1204	210.0	226.83	7.20	6.96	7.40	1007	0.0390 ± 0.0008
798	8.0	222.02	7.30	7.07	7.52	1211	0.0388 ± 0.0009
827	22.0	220.26	7.44	7.20	7.65	1211	0.0392 ± 0.0006
874	44.2	217.75	7.61	7.39	7.75	1211	0.0395 ± 0.0006
1070	135.3	218.61	6.39	6.21	6.53	1211	0.0367 ± 0.0009
1160	184.0	225.37	6.60	6.35	6.89	1211	0.0371 ± 0.0007
1204	210.0	226.83	7.20	6.96	7.40	1211	0.0389 ± 0.0007

Table 1. Summary of thermal conductivity measurements performed by the HP³ instrument in the final measurement configuration following Sol 754. The mission Sol number, the corresponding martian solar longitude (L_s), soil temperature at the beginning of the experiment T_0 , average (P_{avr}), minimum (P_{min}) and maximum (P_{max}) atmospheric pressure during the measurement, as well as the assumed soil density ρ are given together with the determined thermal conductivity k . Stated error bars represent 1- σ confidence intervals and results are shown for the two densities considered.

223 pected for unconsolidated soils, we have converted average diurnal atmospheric pressure
 224 for each measurement to a thermal conductivity estimate using Eqn. 3. Choosing the
 225 thermal conductivity derived for Sol 798 to fix $k_0(P)$, soil thermal conductivity can be
 226 estimated as a function of L_s by first calculating the average diurnal atmospheric pres-
 227 sure using Eqn. 2, and then calculating the expected conductivity change with respect
 228 to $k_0(P)$ using Eqn. 3. The result of this calculation is shown as the solid line in Fig.
 229 3 (Morgan et al., 2018). In addition, the gray-shaded area corresponds to the range of
 230 conductivities predicted including the diurnal pressure fluctuations. As is evident from
 231 the figure, the measured soil thermal conductivities closely follow model predictions, in-
 232 dicating that there is a clear positive correlation of thermal conductivity and atmospheric

233 pressure, i.e., increased atmospheric pressure results in increased soil thermal conduction
 234 and vice versa.

235 **4 Discussion**

236 We have conducted the first long-term in-situ monitoring of martian soil thermal
 237 conductivity using the HP³ mole as a modified line heat source. We find that soil thermal
 238 conductivity at the InSight landing site correlates with atmospheric pressure and
 239 follows the trend predicted by laboratory experiments for unconsolidated soils (Presley
 240 & Christensen, 1997). For the conducted experiments, pressure variations of 1.2 mbar
 241 resulted in conductivity changes of close to 8% , corresponding to approximately 6.5%
 242 mbar⁻¹. This is consistent with model predictions and indicates that a significant frac-
 243 tion of heat transport occurs through the pore-filling gas.

244 Any cementation or induration of the soil would have a significant influence on ther-
 245 mal properties by increasing the contact area between individual grains (Piqueux & Chris-
 246 tensen, 2009a) and this does not seem to be the case for the soil sampled by the HP³ mole.
 247 Even small amounts of cement would result in a significant increase of heat transport
 248 through the grain matrix and the pressure dependence of thermal conductivity would
 249 be minimal (Piqueux & Christensen, 2009b). Therefore, thermal measurements indicate
 250 that the sampled soil is unconsolidated.

251 Some support for the conclusion that soil cementation should be minimal is pro-
 252 vided by the analysis of seismic velocities in the shallow subsurface. Using the HP³ ham-
 253 mering mechanism as a seismic source, Brinkman et al. (2022) determined P-wave v_P
 254 and S-wave v_S velocities in the upper few tens of centimeters of the soil. They found ve-
 255 locities of $v_P = 119^{+45}_{-21}$ m s⁻¹ and $v_S = 63^{+11}_{-7}$ m s⁻¹, consistent with values typically
 256 encountered in low-density unconsolidated sands. It has also been speculated that any
 257 cement at grain contacts within sediment layer at the InSight landing site may have been
 258 broken up by impacts or marsquakes (Wright et al., 2022), although this may be more
 259 relevant for deeper soil layers not probed by the HP³ mole.

260 Nagihara et al. (2022) studied the dependence of thermal conductivity on atmo-
 261 spheric pressure in the lab using the low-cohesion Mojave Mars simulant (Peters et al.,
 262 2008) as an analogue for the martian soil. The simulant is made from crushed basalt with
 263 grain sizes ranging from 0.05 mm to 1 mm and a median grain size of 0.2 mm, compa-

264 rable to the values derived for the landing site (Grott et al., 2021). Cohesion of the sim-
265 ulant is low and smaller than 2 kPa. Experiments were conducted at two different soil
266 densities of 1540 kg m^{-3} and 1660 kg m^{-3} and atmospheric pressure was varied between
267 2 and 10 mbar. While absolute thermal conductivity of the simulant was larger than that
268 determined for the soil at the InSight landing site, which may be attributed to the larger
269 density of the simulant when compared to the in-situ measurements, Nagihara et al. (2022)
270 found the pressure dependence of thermal conductivity to be similar to the one reported
271 here. Over a pressure range of 6 to 10 mbar, the simulant's thermal conductivity increased
272 by 20%, corresponding to $5\% \text{ mbar}^{-1}$ and thus being comparable to the $6.5\% \text{ mbar}^{-1}$
273 observed here.

274 The pressure dependence of the observed soil thermal conductivity is very pronounced
275 and even appears to be slightly larger than predicted by the model of Morgan et al. (2018).
276 In the transitional flow regime relevant to the range of Knudsen numbers encountered
277 in the martian soil, the pressure dependence of thermal conductivity is stronger if pore
278 spaces are smaller. Laboratory measurements on glass beads (Presley & Christensen, 1997)
279 indicate that the observed conductivity changes of about $6.5\% \text{ mbar}^{-1}$ are obtained if
280 particles are dust sized with diameters close to $10 \mu\text{m}$, while larger particles show a weaker
281 dependency of thermal conductivity on atmospheric pressure. The observed pronounced
282 seasonal trend of soil thermal conductivity therefore indicates that a significant fraction
283 of the pore-space is likely filled by dust-sized particles. In addition to explaining the strong
284 dependence of conductivity on atmospheric pressure, dust filled pores could add signif-
285 icant cohesion to the soil.

286 While thermal conductivity measurements thus clearly indicate that soil cemen-
287 tation or induration should be minimal, this is difficult to reconcile with image data that
288 show steep sided pits with pebbles in a finer matrix as well as cohesion estimates that
289 have been derived using the lander's robotic arm (Golombek, Warner, et al., 2020; Marteau
290 et al., 2021). These data strongly suggest a duricrust to be present, which could have
291 been generated by the deposition of salts due to soil-atmosphere interactions (Mutch et
292 al., 1977; Ditteon, 1982; Moore et al., 1999; Banin et al., 1992; Haskin et al., 2005; Huowitz
293 et al., 2006). Furthermore, experimental studies have shown that granular materials be-
294 have more cohesively when tested under vacuum (Salisbury et al., 1964; Bromwell, 1966;
295 Grossman et al., 1970) and reduced-gravity conditions (Kleinhans et al., 2011; White &
296 Klein, 1990; Walton et al., 2007; Elekes & Parteli, 2021), which suggests an enhanced

297 cohesive behavior of the soil under Martian atmospheric pressure and gravity. The pen-
 298 etration data gathered by the HP³ mole also indicates significant penetration resistance
 299 of the soil (Spohn et al., 2022).

300 This discrepancy may be resolved when considering the history of probe emplace-
 301 ment. During the initial penetration attempts, the soil was significantly disrupted and
 302 a hole up to 7 cm deep was created around the mole. This was later back-filled by loose
 303 material, but the duricrust in this depth range has been disaggregated into sand (Spohn
 304 et al., 2022). At larger depth, some soil may also have been disrupted, but the amount
 305 of modified material is estimated to be minor when compared to the volume sampled by
 306 the heat pulse generated in the thermal conductivity experiments, which extends to ap-
 307 proximately 2 to 3 mole diameters (see above). Therefore, the soil properties derived here
 308 should correspond to the unconsolidated soil layers surrounding the mole at larger depths
 309 rather than the duricrust closer to the surface.

310 The existence of gas exchange between soil and the martian atmosphere has been
 311 inferred from models of the martian climate (e.g., Martínez et al. (2017); Buhler & Piqueux
 312 (2021)), models for regolith-water exchange (e.g., Savijärvi et al. (2016)), models for the
 313 transport of trace gases (e.g., Bullock et al. (1994)), as well as models for barometric pump-
 314 ing (de Beule et al., 2014). Furthermore, the exchange and adsorption of gases has been
 315 studied in the lab (e.g., Fanale et al. (1982); Fanale et al. (1982); Rannou et al. (2001)).
 316 However, to our knowledge, the thermal conductivity data presented here is the first di-
 317 rect evidence that the atmosphere interacts with the top most meter of material on Mars.

318 5 Conclusions

319 Soil thermal conductivity at the InSight landing site strongly correlates with at-
 320 mospheric pressure and conductivities vary by 6.5% mbar⁻¹. This is within the range
 321 predicted by models of thermal conductivity as a function of pressure for unconsolidated
 322 soils (Morgan et al., 2018) and consistent with the results of laboratory experiments un-
 323 der martian atmospheric conditions (Presley & Christensen, 1997; Nagihara et al., 2022).
 324 Furthermore, the observed strong correlation between thermal conductivity and atmo-
 325 spheric pressure indicates that pore spaces may be filled with dust sized particles, which
 326 could result in significant soil cohesion.

327 Both the rather low absolute value of thermal conductivity of around 0.038 W m^{-1}
 328 K^{-1} as well as the observed strong pressure dependence of $6.5\% \text{ mbar}^{-1}$ indicate that
 329 the soil probed by the HP³ experiment is unconsolidated. Cementation or induration would
 330 significantly increase grain-to-grain contacts and thus increase the absolute conductiv-
 331 ity by a large factor while at the same time removing the pressure dependence (Piqueux
 332 & Christensen, 2009b). We conclude that the thermal properties derived here are rep-
 333 resentative for the deeper, unconsolidated soil layers rather than the undisturbed duri-
 334 crust observed in image data.

335 Data Availability Statement

336 Calibrated HP³ heating experiment data are archived in NASA's Planetary Data
 337 System (InSight HP3 Science Team, 2021). The numerical code and data necessary to
 338 reproduce the results and figures of this paper have been made publicly available in Grott
 339 (2022).

340 Acknowledgments

341 The design, building of and research into the HP³ has been supported by the German
 342 Aerospace Center DLR, by NASA, the ÖAW, and the Polish Academy of Science. US
 343 government support is gratefully acknowledged. This research was carried out in part
 344 at the Jet Propulsion Laboratory, California Institute of Technology, under a contract
 345 with the National Aeronautics and Space Administration (80NM0018D0004). This pa-
 346 per is InSight Contribution Number 306.

347 References

- 348 Banerdt, W. B., Smrekar, S. E., Banfield, D., Giardini, D., Golombek, M., Johnson,
 349 C. L., ... Wieczorek, M. (2020). Initial results from the InSight mission on Mars.
 350 *Nature Geoscience*, 13(3), 183-189. doi: 10.1038/s41561-020-0544-y
- 351 Banfield, D., Rodriguez-Manfredi, J. A., Russell, C. T., Rowe, K. M., Leneman, D.,
 352 Lai, H. R., ... Banerdt, W. B. (2019). InSight Auxiliary Payload Sensor Suite
 353 (APSS). *Space Science Reviews*, 215(1), 4. doi: 10.1007/s11214-018-0570-x
- 354 Banfield, D., Spiga, A., Newman, C., Forget, F., Lemmon, M., Lorenz, R., ...
 355 Banerdt, W. B. (2020). The atmosphere of Mars as observed by InSight. *Na-*
 356 *ture Geoscience*, 13(3), 190-198. doi: 10.1038/s41561-020-0534-0

- 357 Banin, A., Clark, B. C., & Waenke, H. (1992). Surface chemistry and mineralogy. In
 358 M. George (Ed.), *Mars* (p. 594-625).
- 359 Blackwell, J. H. (1956, April). The Axial-Flow Error in the Thermal-Conductivity
 360 Probe. *Canadian Journal of Physics*, 34(4), 412-417. doi: 10.1139/p56-048
- 361 Brinkman, N., Schmelzbach, C., Sollberger, D., ten Pierick, J., Edme, P., Haag,
 362 T., ... et al. (2022). In-situ regolith seismic velocity measurement at the in-
 363 sight landing site on mars. *Earth and Space Science Open Archive*, 32. doi:
 364 10.1002/essoar.10512064.1
- 365 Bromwell, L. G. (1966). *The friction of quartz in high vacuum* (Tech. Rep. No. 3-
 366 101). Department of Civil Engineering, M.I.T. Cambridge, MA: Research In Earth
 367 Physics, Phase Report No. 7.
- 368 Buhler, P., & Piqueux, S. (2021). Obliquity-driven CO₂ exchange between mars'
 369 atmosphere, regolith, and polar cap. *Journal of Geophysical Research: Planets*,
 370 126(5). doi: 10.1029/2020JE006759
- 371 Bullock, M. A., Stoker, C. R., McKay, C. P., & Zent, A. P. (1994, January). A Cou-
 372 pled Soil-Atmosphere Model of H₂O₂ on Mars. *Icarus*, 107(1), 142-154. doi: 10
 373 .1006/icar.1994.1012
- 374 Carslaw, H., & Jaeger, J. (1959). Conduction of heat in solids. In (Second ed.,
 375 chap. 13). London: Oxford at the Clarendon Press.
- 376 Compaire, N., Margerin, L., Monnereau, M., Garcia, R. F., Lange, L., Calvet, M.,
 377 ... Banerdt, W. B. (2022, May). Seasonal variations of subsurface seismic veloc-
 378 ities monitored by the SEIS-InSight seismometer on Mars. *Geophysical Journal
 379 International*, 229(2), 776-799. doi: 10.1093/gji/ggab499
- 380 de Beule, C., Wurm, G., Kelling, T., Küpper, M., Jankowski, T., & Teiser, J. (2014).
 381 The martian soil as a planetary gas pump. *Nature Physics*, 10(1), 17-20. doi: 10
 382 .1038/nphys2821
- 383 Ditteon, R. (1982). Daily temperature variations on Mars. *Journal of Geophysical
 384 Research*, 87, 10197-10214. doi: 10.1029/JB087iB12p10197
- 385 Edgett, K. S., Yingst, R. A., Minitti, M. E., Goetz, W., Kah, L. C., Kennedy,
 386 M. R., ... MSL Science Team (2013, March). Mars Hand Lens Imager (MAHLI)
 387 Efforts and Observations at the “Rocknest” Eolian Sand Shadow in Curiosity’s
 388 Gale Crater Field Site. In *Lunar and planetary science conference* (p. 1201).
- 389 Elekes, F., & Parteli, E. J. R. (2021, September). An expression for the angle of

- 390 repose of dry cohesive granular materials on Earth and in planetary environments.
- 391 *Proceedings of the National Academy of Science*, 118(38), e2107965118. doi:
392 10.1073/pnas.2107965118
- 393 Fanale, F. P., Banerdt, W. B., Saunders, R. S., Johansen, L. A., & Salvail, J. R.
394 (1982). Seasonal carbon dioxide exchange between the regolith and atmo-
395 sphere of mars: Experimental and theoretical studies. *Journal of Geophysical
396 Research: Solid Earth*, 87(B12), 10215-10225. doi: <https://doi.org/10.1029/JB087iB12p10215>
- 398 Fanale, F. P., Salvail, J. R., Banerdt, W. B., & Saunders, R. S. (1982, June). Mars:
399 The regolith-atmosphere-cap system and climate change. *Icarus*, 50(2-3), 381-407.
400 doi: 10.1016/0019-1035(82)90131-2
- 401 Fergason, R., Christensen, P., Bell, J., Golombek, M., Herkenhoff, K., & Kieffer,
402 H. (2006). Physical properties of the Mars Exploration Rover landing sites as
403 inferred from Mini-TES-derived thermal inertia. *Journal of Geophysical Research
404 (Planets)*, 111(E2), E02S21. doi: 10.1029/2005JE002583
- 405 Golombek, M., Warner, N. H., Grant, J. A., Hauber, E., Ansan, V., Weitz, C. M.,
406 ... Banerdt, W. B. (2020). Geology of the InSight landing site on Mars. *Nature
407 Communications*, 11, 1014. doi: 10.1038/s41467-020-14679-1
- 408 Golombek, M., Williams, N., Warner, N. H., Parker, T., Williams, M. G., Daubar,
409 I., ... Sklyanskiy, E. (2020). Location and Setting of the Mars InSight Lander,
410 Instruments, and Landing Site. *Earth and Space Science*, 7(10), e01248. doi:
411 10.1029/2020EA001248
- 412 Grossman, J. J., Ryan, J. A., Mukherjee, N. R., & Wegner, M. W. (1970, January).
413 Micro-chemical, microphysical and adhesive properties of lunar material. *Geochim-
414 ica et Cosmochimica Acta Supplement*, 1, 2171.
- 415 Grott, M. (2022). Supplementary Material for "Seasonal Variations of Soil Thermal
416 Conductivity at the InSight Landing Site". *Figshare Collection*. doi: <https://doi.org/10.6084/m9.figshare.c.6359816>
- 418 Grott, M., Spohn, T., Knollenberg, J., Krause, C., Hudson, T. L., Piqueux, S., ...
419 Banerdt, W. B. (2021). Thermal Conductivity of the Martian Soil at the InSight
420 Landing Site From HP³ Active Heating Experiments. *Journal of Geophysical
421 Research (Planets)*, 126(7), e06861. doi: 10.1029/2021JE006861
- 422 Grott, M., Spohn, T., Knollenberg, J., Krause, C., Scharringhausen, M., Wipper-

- 423 mann, T., ... Banerdt, W. B. (2019). Calibration of the Heat Flow and Physical
424 Properties Package (HP³) for the InSight Mars Mission. *Earth and Space Science*,
425 6(12), 2556-2574. doi: 10.1029/2019EA000670
- 426 Hamilton, V. E., Vasavada, A. R., Sebastián, E., Torre Juárez, M., Ramos, M.,
427 Armiens, C., ... Zorzano, M.-P. (2014). Observations and preliminary science
428 results from the first 100 sols of MSL Rover Environmental Monitoring Station
429 ground temperature sensor measurements at Gale Crater. *Journal of Geophysical
430 Research (Planets)*, 119(4), 745-770. doi: 10.1002/2013JE004520
- 431 Hammerschmidt, U., & Sabuga, W. (2000). Transient hot wire (THW) method: Un-
432 certainty Assessment. *Intern. J. Thermophys.*, 21(6), 1225-1278.
- 433 Haskin, L. A., Wang, A., Jolliff, B. L., McSween, H. Y., Clark, B. C., Des Marais,
434 D. J., ... Soderblom, L. (2005). Water alteration of rocks and soils on
435 Mars at the Spirit rover site in Gusev crater. *Nature*, 436(7047), 66-69. doi:
436 10.1038/nature03640
- 437 Hecht, M. H., Kounaves, S. P., Quinn, R. C., West, S. J., Young, S. M. M., Ming,
438 D. W., ... Smith, P. H. (2009). Detection of Perchlorate and the Soluble Chem-
439 istry of Martian Soil at the Phoenix Lander Site. *Science*, 325(5936), 64. doi:
440 10.1126/science.1172466
- 441 Huetter, E. S., Koemle, N. I., Kargl, G., & Kaufmann, E. (2008, December). De-
442 termination of the effective thermal conductivity of granular materials under
443 varying pressure conditions. *Journal of Geophysical Research (Planets)*, 113(E12),
444 E12004. doi: 10.1029/2008JE003085
- 445 Hurowitz, J. A., McLennan, S. M., Tosca, N. J., Arvidson, R. E., Michalski, J. R.,
446 Ming, D. W., ... Squyres, S. W. (2006). In situ and experimental evidence for
447 acidic weathering of rocks and soils on Mars. *Journal of Geophysical Research
448 (Planets)*, 111(E2), E02S19. doi: 10.1029/2005JE002515
- 449 InSight HP3 Science Team. (2021). Mars InSight Lander HP³ Data Archive. *Plane-
450 tary Data System*. doi: 10.17189/1517573
- 451 Jaeger, J. C. (1956). Conduction of Heat in an Infinite Region Bounded Internally
452 by a Circular Cylinder of a Perfect Conductor. *Australian Journal of Physics*, 9,
453 167. doi: 10.1071/PH560167
- 454 Kleinhans, M. G., Markies, H., de Vet, S. J., in't Veld, A. C., & Postema, F. N.
455 (2011, November). Static and dynamic angles of repose in loose granular materi-

- als under reduced gravity. *Journal of Geophysical Research (Planets)*, 116(E11), E11004. doi: 10.1029/2011JE003865
- Kounaves, S. P., Chaniotakis, N. A., Chevrier, V. F., Carrier, B. L., Folds, K. E., Hansen, V. M., ... Weber, A. W. (2014). Identification of the perchlorate parent salts at the Phoenix Mars landing site and possible implications. *Icarus*, 232, 226-231. doi: 10.1016/j.icarus.2014.01.016
- Lange, L., Forget, F., Banfield, D., Wolff, M., Spiga, A., Millour, E., ... Banerdt, W. B. (2022, May). InSight Pressure Data Recalibration, and Its Application to the Study of Long-Term Pressure Changes on Mars. *Journal of Geophysical Research (Planets)*, 127(5), e07190. doi: 10.1029/2022JE007190
- Martéau, E., Golombek, M., Vrettos, C., & Garvin, J. (2021). Soil Mechanical Properties at the InSight Landing Site on Mars. In *Lunar and planetary science conference* (p. 2067).
- Martínez, G. M., Newman, C. N., De Vicente-Retortillo, A., Fischer, E., Renno, N. O., Richardson, M. I., ... Vasavada, A. R. (2017, October). The Modern Near-Surface Martian Climate: A Review of In-situ Meteorological Data from Viking to Curiosity. *Space Science Reviews*, 212(1-2), 295-338. doi: 10.1007/s11214-017-0360-x
- Mellon, M. T., Arvidson, R. E., Sizemore, H. G., Searls, M. L., Blaney, D. L., Cull, S., ... Zent, A. P. (2009). Ground ice at the phoenix landing site: Stability state and origin. *Journal of Geophysical Research: Planets*, 114(E1). doi: <https://doi.org/10.1029/2009JE003417>
- Moore, H. J., Bickler, D. B., Crisp, J. A., Eisen, H. J., Gensler, J. A., Haldemann, A. F. C., ... Pavlcs, F. (1999). Soil-like deposits observed by Sojourner, the Pathfinder rover. *Journal of Geophysical Research*, 104(E4), 8729-8746. doi: 10.1029/1998JE900005
- Morgan, P., Grott, M., Knapmeyer-Endrun, B., Golombek, M., Delage, P., Lognonné, P., ... Kedar, S. (2018). A Pre-Landing Assessment of Regolith Properties at the InSight Landing Site. *Space Science Reviews*, 214(6), 104. doi: 10.1007/s11214-018-0537-y
- Mueller, N. T., Knollenberg, J., Grott, M., Kopp, E., Walter, I., Krause, C., ... Smrekar, S. (2020). Calibration of the HP³ Radiometer on InSight. *Earth and Space Science*, 7(5), e01086. doi: 10.1029/2020EA001086

- 489 Mueller, N. T., Piqueux, S., Lemmon, M., Maki, J., Lorenz, R., Grott, M., ...
490 Banerdt, W. (2021). Near surface properties derived from Phobos transits with
491 HP³ RAD on InSight, Mars. *Geophysical Research Letters*, submitted.
492 Mutch, T. A., Arvidson, R. E., Binder, A. B., Guinness, E. A., & Morris, E. C.
493 (1977). The geology of the Viking lander 2 site. *Journal of Geophysical Research*,
494 82(B28), 4452-4467. doi: 10.1029/JB082i028p04452
495 Nagihara, S., Ngo, P., & Grott, M. (2022). Thermal Properties of the Mojave Mars
496 Regolith Simulant in Mars-Like Atmospheric Conditions. *International Journal of*
497 *Thermophysics*, 43(7), 98. doi: 10.1007/s10765-022-03023-y
498 Peters, G. H., Abbey, W., Bearman, G. H., Mungas, G. S., Smith, J. A., Ander-
499 son, R. C., ... Beegle, L. W. (2008). Mojave Mars simulant—Characterization
500 of a new geologic Mars analog. *Icarus*, 197(2), 470-479. doi: 10.1016/
501 j.icarus.2008.05.004
502 Piqueux, S., & Christensen, P. R. (2009a). A model of thermal conductivity for
503 planetary soils: 1. Theory for unconsolidated soils. *Journal of Geophysical Re-*
504 *search (Planets)*, 114(E9), E09005. doi: 10.1029/2008JE003308
505 Piqueux, S., & Christensen, P. R. (2009b). A model of thermal conductivity for
506 planetary soils: 2. Theory for cemented soils. *Journal of Geophysical Research*
507 (*Planets*), 114(E9), E09006. doi: 10.1029/2008JE003309
508 Presley, M. A., & Christensen, P. R. (1997). The effect of bulk density and particle
509 size sorting on the thermal conductivity of particulate materials under Martian
510 atmospheric pressures. *Journal of Geophysical Research (Planets)*, 102(E4),
511 9221-9230. doi: 10.1029/97JE00271
512 Presley, M. A., Craddock, R. A., & Zolotova, N. (2009). The effect of salt crust on
513 the thermal conductivity of one sample of fluvial particulate materials under Mar-
514 tian atmospheric pressures. *Journal of Geophysical Research (Planets)*, 114(E11),
515 E11007. doi: 10.1029/2009JE003355
516 Rannou, P., Chassefière, E., Encrenaz, T., Erard, S., Génin, J., Ingrin, J., ... Tou-
517 blanc, D. (2001). Exocam: Mars in a box to simulate soil-atmosphere interac-
518 tions. *Advances in Space Research*, 27(2), 189-193. doi: https://doi.org/10.1016/
519 S0273-1177(01)00046-1
520 Salisbury, J. W., Glaser, P. E., Stein, B. A., & Vonnegut, B. (1964, January). Ad-
521 hesive Behavior of Silicate Powders in Ultrahigh Vacuum. *Journal of Geophysical*

- 522 *Research*, 69(2), 235-242. doi: 10.1029/JZ069i002p00235
- 523 Savijärvi, H., Harri, A.-M., & Kemppinen, O. (2016). The diurnal water cycle at
524 Curiosity: Role of exchange with the regolith. *Icarus*, 265, 63-69. doi: 10.1016/j.
525 .icarus.2015.10.008
- 526 Spiga, A., Banfield, D., Teanby, N. A., Forget, F., Lucas, A., Kenda, B., ...
527 Banerdt, W. B. (2018). Atmospheric Science with InSight. *Space Science Re-*
528 *views*, 214(7), 109. doi: 10.1007/s11214-018-0543-0
- 529 Spohn, T., Grott, M., Smrekar, S. E., Knollenberg, J., Hudson, T. L., Krause, C.,
530 ... Banerdt, W. B. (2018). The Heat Flow and Physical Properties Pack-
531 age (HP³) for the InSight Mission. *Space Science Reviews*, 214(5), 96. doi:
532 10.1007/s11214-018-0531-4
- 533 Spohn, T., Hudson, T. L., Marteau, E., Golombek, M., Grott, M., Wippermann, T.,
534 ... Banerdt, W. B. (2022). The InSight HP³ Penetrator (Mole) on Mars: Soil
535 Properties Derived from the Penetration Attempts and Related Activities. *Space*
536 *Science Reviews*, 218(8), 72. doi: 10.1007/s11214-022-00941-z
- 537 Spohn, T., Hudson, T. L., Witte, L., Wippermann, T., Wisniewski, L., Kedziora, B.,
538 ... Grygorczuk, J. (2022). The InSight-HP³ mole on Mars: Lessons learned from
539 attempts to penetrate to depth in the Martian soil. *Advances in Space Research*,
540 69(8), 3140-3163. doi: <https://doi.org/10.1016/j.asr.2022.02.009>
- 541 von Herzen, R., & Maxwell, A. E. (1959). The Measurement of Thermal Conductiv-
542 ity of Deep-Sea Sediments by a Needle-Probe Method. *Journal of Geophysical Re-*
543 *search*, 64(10), 1557-1563. doi: 10.1029/JZ064i010p01557
- 544 Walton, O., De Moor, C., & Gill, K. (2007). Effects of gravity on cohesive behav-
545 ior of fine powders: implications for processing Lunar regolith. *Granular Matter*,
546 9, 353–363. doi: 10.1007/s10035-006-0029-8
- 547 White, B. R., & Klein, S. P. (1990, October). Dynamic shear of granular mate-
548 rial under variable gravity conditions. *AIAA Journal*, 28(10), 1701-1702. doi: 10
549 .2514/3.10461
- 550 Wright, V., Dasent, J., Kilburn, R., & Manga, M. (2022). A minimally ce-
551 mented shallow crust beneath insight. *Geophysical Research Letters*, 49(15),
552 e2022GL099250. doi: <https://doi.org/10.1029/2022GL099250>
- 553 Yingst, R. A., Kah, L. C., Palucis, M., Williams, R. M. E., Garvin, J., Bridges,
554 J. C., ... Wiens, R. C. (2013). Characteristics of pebble- and cobble-sized clasts

555 along the Curiosity rover traverse from Bradbury Landing to Rocknest. *Journal of*
556 *Geophysical Research (Planets)*, 118(11), 2361-2380. doi: 10.1002/2013JE004435
557 Zent, A. P., Hecht, M. H., Cobos, D. R., Wood, S. E., Hudson, T. L., Milkovich,
558 S. M., ... Mellon, M. T. (2010). Initial results from the thermal and electri-
559 cal conductivity probe (TECP) on Phoenix. *Journal of Geophysical Research*
560 (*Planets*), 115(2), E00E14. doi: 10.1029/2009JE003420

Figure 1.

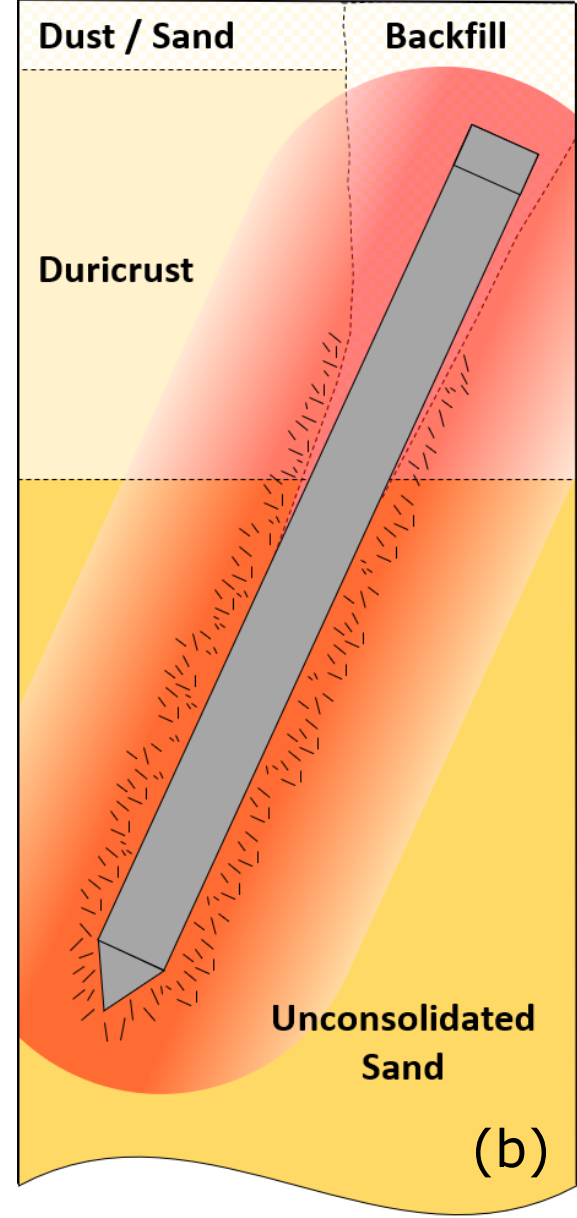
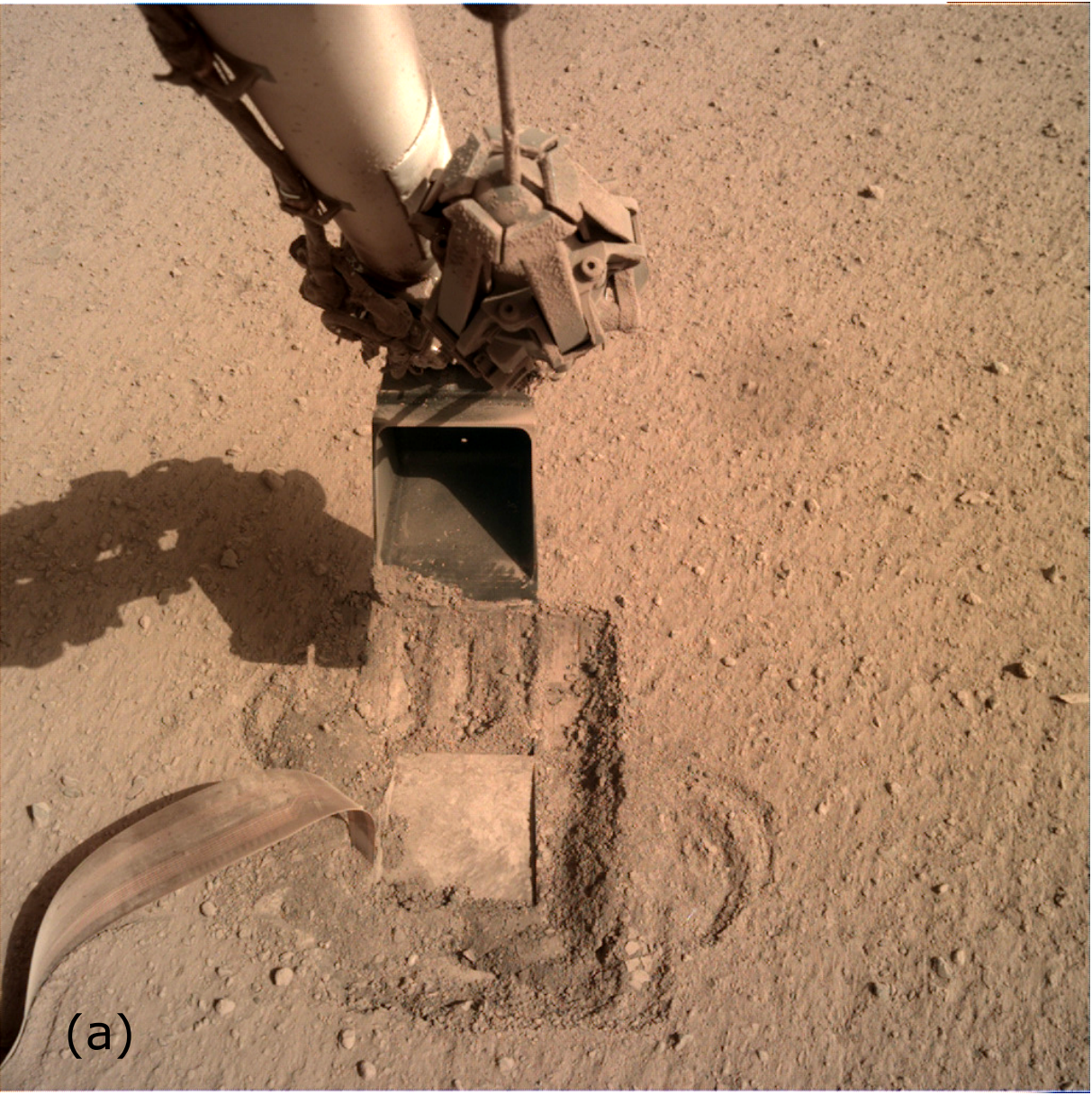


Figure 2.

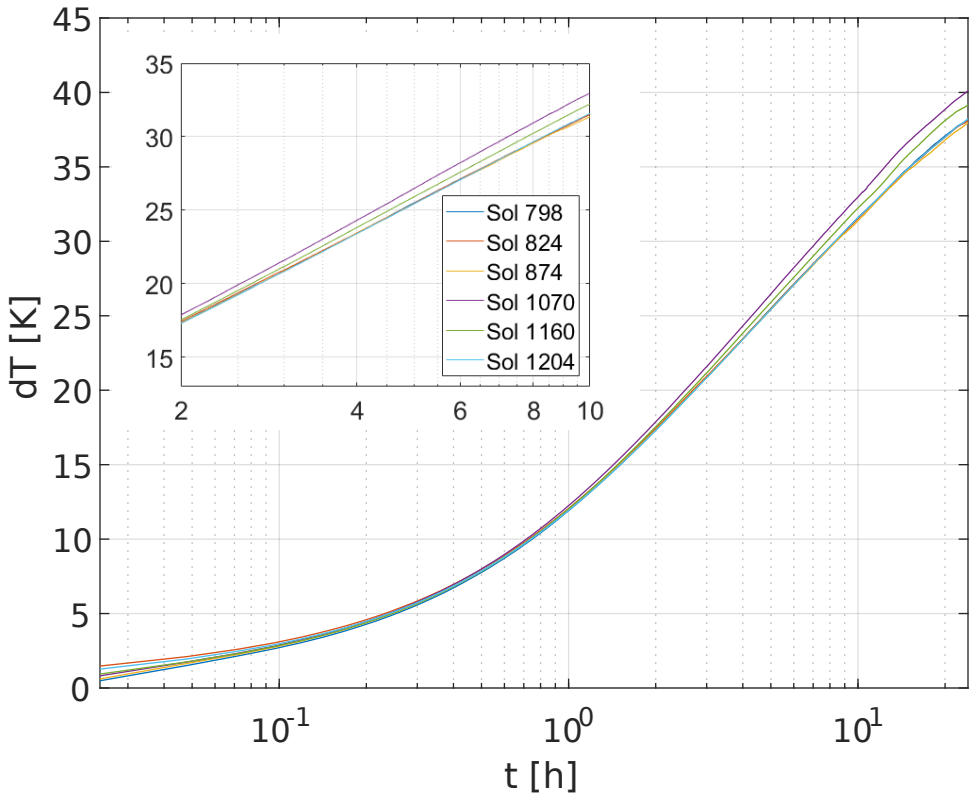


Figure 3.

